Inorganic Chemistry

Article

pubs.acs.org/IC

Mn_8 Cluster with Ferrocene-1,1′-Dicarboxylate Ligation: Single-Molecule Magnetism with Multiple External Redox Centers

Antonio Masello,[†] Khalil A. Abboud,[†] Wolfgang Wernsdorfer,[‡] and George Christou*[,†]

[†]Department of Chemistry, University of Florida, Gainesville, Florida 32611-7200, United States

[‡]Institut Néel, CNRS/UJP, BP 166, 38042 Grenoble Cedex 9, France

Supporting Information

ABSTRACT: The syntheses, structures, and magnetic properties are reported of a new Mn_8 cluster obtained from the reaction of ferrocene-1,1′-dicarboxylic acid ($fdcH_2$) with $[Mn_{12}O_{12}(O_2CMe)_{16}(H_2O)_4]$ and mononuclear Mn salts under different conditions and limited light exposure. The product was obtained in two forms: $[Mn_8O_4(fdc)_6(DMF)_2(H_2O)_2]$ (**1**) and $[Mn_8O_4(fdc)_6(DMF)_4]$ (**2**), differing in the bound solvent ligands. The structures are otherwise almost identical, comprising very similar cores that both contain $4Mn^{III}$ and $4Mn^{II}$ atoms bridged by four O^{2-} ions and six fdc^{2-} groups. The $[Mn^{III}_4Mn^{II}_4(\mu_4\text{-}O)_4]$ cores have virtual T_d symmetry and can be described as a central $[Mn^{III}_4(\mu_4\text{-}O)_4]^{4+}$ cubane unit whose four O^{2-} ions are μ_4, because they each attach to an external Mn^{II} atom. Peripheral ligation about the core is provided by six bridging fdc^{2-} groups and the terminal solvent ligands, one each on the Mn^{II} atoms. The differences in solvent ligands between **1** and **2**, and different packing from the different crystal space groups, lead to significant differences in metric parameters within the core, which are reflected in significantly different magnetic properties. Variable-temperature, solid-state dc and ac susceptibility measurements reveal the clusters to be predominantly antiferromagnetically coupled, and to possess ground state spin values of $S = 5$ and $S = 2$ for **1** and **2**, respectively. The difference in ground states is assigned to the small but distinct structural differences seen in the central cubane. Alternating current (AC) susceptibility data indicate **1** and **2** to be new single-molecule magnet, and this was confirmed by magnetization versus direct current (DC) field scans on a single crystal of **1**·4DMF·$4H_2O$, which exhibited hysteresis.

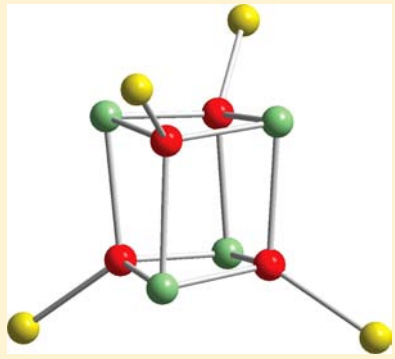

INTRODUCTION

Many oxo-bridged transition-metal clusters of 3d metals display interesting physicochemical properties that, in some cases, include the unusual magnetic behavior that has come to be known as single-molecule magnetism.[1−4] The coexistence in such clusters of a large ground-state spin (S) with a large and negative axial magnetic anisotropy (D) can lead to them being single-molecule magnets (SMMs) below a characteristic blocking temperature T_B. SMMs behave as molecular superparamagnets exhibiting slow magnetization relaxation and, consequently, magnetic hysteresis below T_B, as a consequence of a sufficiently large (vs kT) energy barrier (U) to the reversal of the magnetization vector along the easy axis (z-axis).[2] As this area has expanded, various synthetic methods have been devised and many different types of SMMs have been discovered, spanning a wide variety of metal nuclearities, topologies, and ligand types. Most of these have been in Mn or Ln (Ln = lanthanide) chemistry, or in the heterometallic cluster chemistry of the two together.[1,3,5−8] The high magnetic anisotropy of many lanthanides has proven highly beneficial to this area and has been the focus of increased interest over the past few years. Nevertheless, Mn chemistry remains a major source of SMMs, primarily due to the anisotropy resulting from the Jahn−Teller distortion in octahedral high-spin Mn^{III}, the common occurrence of O^{2-} bridges in Mn^{III}-containing clusters that lead to exchange couplings of significant strength, and the remarkable propensity of Mn-oxo chemistry to give clusters with a myriad of nuclearities and topologies.

In the present work, we have explored the reaction of Mn sources with the ligand precursor ferrocene-1,1′-dicarboxylic acid ($fdcH_2$) as a potential means to new clusters possessing SMM properties while carrying multiple redox-active ligands.

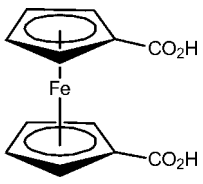

$fdcH_2$

The component fdc^{2-} is an unusual dicarboxylate that has two connected carboxylate groups but, nevertheless, has a significant flexibility in its binding mode imparted by the ability of its cyclopentadienyl rings to rotate about the Cp−Fe−Cp axis, varying the torsion angle between the carboxylates. While fdc^{2-} has been used widely in coordination chemistry to

Received: May 14, 2013
Published: August 23, 2013

   dx.doi.org/10.1021/ic4011955 | *Inorg. Chem.* 2013, 52, 10414−10423

date,[9−13] its incorporation into Mn clusters is still poorly explored. Together with the one-electron redox ability of the ferrocenyl unit, this suggested that fdc^{2-} might provide access to structural types not accessible with simple carboxylates or more-rigid dicarboxylates, and that these could also exhibit multiple redox processes that might lead to interesting modulation of the magnetic and other properties of the clusters obtained. This dual function of the redox active fdc^{2-} group thus distinguishes it from previous work of incorporating organic redox ligands around a Mn cluster, such as the introduction of 16 organic radical ligands into the $[Mn_{12}O_{12}(O_2CR)_{16}(H_2O)_4]$ SMM.[14] For this purpose, we thus have concentrated our efforts on obtaining products with only fdc^{2-} ligation around the core, other than solvent-derived ligands. This has proved to be an interesting but challenging area, because of two recurring problems: (i) products are usually highly insoluble, and (ii) the yields of characterizable materials are very low. These two factors have severely hampered our efforts to push this area forward. However, in a preliminary report, we described access to three molecular clusters: $[Mn_7O_3(OMe)(fdc)_6(H_2O)_3]$, $[Mn_8O_4(fdc)_6(DMF)_2(H_2O)_2]$ (denoted as **1**; DMF = *N*,*N*-dimethylformamide), and $[Mn_{13}O_8(OMe)_6(fdc)_6]$.[15] The Mn_{13} product was a known species obtained by Kondo and co-workers from a different synthetic procedure,[16] but the Mn_7 and Mn_8 products were new in metal fdc^{2-} chemistry; however, the yields were very low, the Mn_8 product being obtained only in 2% yield. More recently, there have been reports of fdc^{2-} being used in conjunction with other ligand types to prepare mixed-ligand 3d−4f complexes,[17,18] a distinctly different strategy from the one we are using, as well as the complexes with an *N*,*N*-based ferrocene chelating ligand.[19] We herein report the synthesis, structures, and magnetic properties of **1** and $[Mn_8O_4(fdc)_6(DMF)_4]$ (**2**), which represent a single-molecule magnet with multiple ferrocenyl redox units as peripheral ligands. We shall also report an excellent, high-yield synthesis of **2** that has been discovered, and how small structural differences between **1** and **2** lead to surprisingly large differences in their magnetic properties.

EXPERIMENTAL SECTION

Syntheses. All preparations were performed in the dark under aerobic conditions and in ambient temperature. All chemicals were used as-received. $[Mn_{12}O_{12}(O_2CMe)_{16}(H_2O)_4]\cdot 2MeCO_2H\cdot 4H_2O$ was prepared as described elsewhere.[20] The reactions and crystallizations were carried in darkness by covering the vessels with aluminum foil.

$[Mn_8O_4(fdc)_6(DMF)_2(H_2O)_2]$ (1): Method A. To a stirred suspension of $fdcH_2$ (0.500 mmol, 0.137 g) in CH_2Cl_2/MeOH (25 mL; 1:1 v/v) was added solid $[Mn_{12}O_{12}(O_2CMe)_{16}(H_2O)_4]\cdot 2MeCO_2H\cdot 4H_2O$ (0.125 mmol, 0.257 g). The mixture was stirred for 1 h and filtered. The copious residue was washed well with CH_2Cl_2/MeOH, and then extracted with DMF (10 mL) with stirring; then, the solution was filtered, and the resulting dark brown filtrate left undisturbed at ambient temperature. Dark brown needles of **1**·4DMF·$4H_2O$ slowly formed over 2 weeks, and these were collected by filtration, washed with a small amount of cold DMF, and dried under vacuum. The yield was ∼2% (∼10 mg). Longer crystallization times led to the appearance of an unknown powder contaminant and were avoided. Vacuum-dried crystals were identified via analysis as **1**·3DMF. Anal. Calcd for $C_{87}H_{87}N_5Mn_8Fe_6O_{35}$: C, 41.18%, H 3.46%, N, 2.76%. Found: C, 41.60%, H 3.59%, N, 2.44%. Selected IR data (KBr pellet, cm^{-1}): 1685 (s), 1577 (vs), 1475 (vs), 1392 (vs), 1537 (vs), 1197 (m), 1029 (m), 923 (w), 829 (w), 798 (w), 780 (m), 635 (m), 517 (s).

$[Mn_8O_4(fdc)_6(DMF)_2(H_2O)_2]$ (1): Method B. To a slurry of $Mn(O_2CMe)_2\cdot 4H_2O$ (0.066 mmol, 16.3 mg) and $fcdH_2$ (0.55 mmol, 0.150 g) in EtOH/py/NEt_3 (20:1:0.7 mL) was added solid $NBu^n_4MnO_4$ (0.026 mmol, 9.5 mg). A dark brown powder of the title compound precipitated within an hour. The powder was collected by filtration, washed well with EtOH, and dried under vacuum. The yield was ∼40% (∼17 mg), and the dried powder was identified via analysis as **1**·3DMF. Anal. Calcd for $C_{87}H_{87}N_5Mn_8Fe_6O_{35}$: C, 41.18%, H 3.46%, N, 2.76%. Found: C, 40.70%, H 3.84%, N, 2.53%. Selected IR data (KBr pellet, cm^{-1}): 1683 (s), 1578 (vs), 1475 (vs), 1389 (vs), 1534 (vs), 1198 (m), 1025 (m), 920 (w), 827 (w), 800 (w), 782 (m), 634 (m), 518 (s).

$[Mn_8O_4(fdc)_6(DMF)_4]$ (2). To an orange solution of $fdcH_2$ (0.500 mmol, 0.137 g) in DMF (10 mL) was added solid $Mn(O_2CMe)_2\cdot 4H_2O$ (0.40 mmol, 0.10 g), and the slurry was stirred until all of the solid had dissolved. Freshly synthesized $[Mn_{12}O_{12}(O_2CMe)_{16}(H_2O)_4]\cdot 2MeCO_2H\cdot 4H_2O$ (0.021 mmol, 0.043 g) was powdered and added slowly as a solid to the stirring solution. The solution was left stirring for 2 h at ambient temperature, giving a dark brown solution and some suspended fine brown powder. The mixture was centrifuged and the supernatant isolated by pipet. Et_2O was slowly layered onto this solution, and X-ray-quality black crystals of **2**·4DMF slowly formed over a few days as the solutions slowly mixed. They were collected by filtration, washed with a small amount of DMF/Et_2O, and dried under vacuum. The yield was ∼85% (0.185 g). The X-ray sample was taken directly from mother liquor. Vacuum-dried crystals were identified via analysis as $\mathbf{2}\cdot{}^3/_2DMF\cdot 3H_2O$. Anal. Calcd for $C_{88.5}H_{92.5}Fe_6N_{5.5}Mn_8O_{36.5}$: C, 41.01%, H 3.60%, N, 2.97%. Found: C, 40.97%, H 3.45%, N, 3.06%. Selected IR data (KBr pellet, cm^{-1}): 1682 (s), 1576 (vs), 1480 (vs), 1389 (vs), 1536 (vs), 1201 (m), 1035 (m), 920 (w), 834 (w), 796 (w), 762 (m), 628 (m), 520 (s).

X-ray Crystallography. Data for **1**·4DMF·$4H_2O$ were collected at 173 K on a Siemens SMART PLATFORM equipped with a CCD area detector and a graphite monochromator utilizing Mo Kα radiation (λ = 0.71073 Å). Cell parameters were refined using 8192 reflections. A full sphere of data (1850 frames) was collected using the ω-scan method (0.3° frame width). The first 50 frames were remeasured at the end of data collection to monitor instrument and crystal stability (maximum correction on I was <1%). Absorption corrections by integration were applied, based on measured indexed crystal faces. The structure was solved by direct methods in SHELXTL6,[21] and refined on F^2 using full-matrix least-squares cycles. The non-hydrogen atoms were refined anisotropically, whereas the hydrogen atoms were calculated in ideal positions and refined as riding on their respective carbon atoms. The asymmetric unit consists of a half cluster, two DMF molecules, one of which is disordered and was refined in two positions, and two H_2O molecules. The H atoms on the bound H_2O (O14) were found and refined freely, whereas those of the interstitial solvent (O17 and O18) were found but were constrained to their respective parent atoms. A total of 670 parameters were included in the final cycle of refinement using 32 126 reflections with $I > 2\sigma(I)$ to yield R_1 = 4.56% and wR_2 = 9.27%.

Data for **2**·4DMF were collected at 100 K on a Bruker SMART diffractometer, using Mo Kα radiation (λ = 0.71073 Å) and an APEXII CCD area detector. Raw data frames were read using the SAINT program[22] and integrated using three-dimensional (3D) profiling algorithms. The resulting data were reduced to produce *hkl* reflections, as well as their intensities and estimated standard deviations. The data were corrected for Lorentz and polarization effects, and numerical absorption corrections were applied based on indexed and measured faces. The structure was solved and refined in SHELXTL6.1,[21] using full-matrix least-squares cycles. The non-hydrogen atoms were refined anisotropically, and all hydrogen atoms were calculated in ideal positions and refined as riding on their parent atoms. The asymmetric unit consists of the Mn_8 cluster and four DMF solvent molecules. The latter were badly disordered and could not be modeled properly; thus, the SQUEEZE program,[23] which is a part of the PLATON[23] package of crystallographic software, was used to calculate the solvent disorder area and remove its contribution to the overall intensity data. One of

dx.doi.org/10.1021/ic4011955 | Inorg. Chem. 2013, 52, 10414−10423

the DMF ligands is disordered in two parts (except for the oxygen atom), and their site occupation factors were dependently refined. A total of 1210 parameters were included in the final cycle of refinement using 23 801 reflections (15 611 of which are observed with $I > 2\sigma(I)$) to yield R_1 = and 4.29% and wR_2 = 9.47%.

Unit-cell data and details of the structure refinement for the two compounds are given in Table 1.

Table 1. Crystallographic Data for 1·4DMF·4H_2O and 2·4DMF

parameter	1·4DMF·4H_2O	2·4DMF
formula[a]	$C_{90}H_{102}N_6Fe_6Mn_8O_{40}$	$C_{96}H_{104}N_8Fe_6Mn_8O_{36}$
formula weight, fw[a]	2682.40 g mol^{-1}	2720.49 g mol^{-1}
crystal system	monoclinic	monoclinic
space group	$C2/c$	$P2_1/c$
a	23.282(3) Å	24.015(2) Å
b	19.331(3) Å	14.8647(14) Å
c	22.198(3) Å	29.558(3) Å
β	97.885(3)°	101.088(5)°
V	9896(3) Å^3	10354.7(17) Å^3
Z	4	4
T	173(2) K	100(2) K
radiation[b]	0.71073 Å	0.71073 Å
ρ_{calc}	1.660 g cm^{-3}	1.745 g cm^{-3}
μ	1.950 mm^{-1}	1.839 mm^{-1}
$R1$[c,d]	0.0456	0.0429
$wR2$[e]	0.0927	0.0947

[a]Including solvent molecules. [b]Graphite monochromator. [c]$I > 2\sigma(I)$. [d]$R1 = \sum(||F_o| - |F_c||)/\sum F_o|$. [e]$wR2 = [\sum[w(F_o^2 - F_c^2)^2]/\sum[w(F_o^2)^2]]^{1/2}$, $w = 1/[\sigma^2(F_o^2) + [(ap)^2 + bp]$, where $p = [\max(F_o^2, 0) + 2F_c^2]/3$.

Other Studies. Infrared (IR) spectra were recorded in the solid state (KBr pellets) on a Nicolet Nexus 670 FTIR spectrometer in the 400−4000 cm^{-1} range. Elemental analyses (C, H, and N) were performed by the in-house facilities in the Chemistry Department at the University of Florida. Metal analyses were obtained from Desert Analytics (Tucson, AZ, USA). Variable-temperature direct current (DC) and alternating current (AC) magnetic susceptibility data were collected on a Quantum Design MPMS-XL SQUID magnetometer equipped with a 7 T magnet and operating in the 1.8−300 K range. Samples were embedded in solid eicosane, to prevent torquing. Magnetization versus field and temperature data were fit using the MAGNET program.[24] Pascal's constants[25] were used to estimate the diamagnetic corrections, which were subtracted from the experimental susceptibilities to give the molar paramagnetic susceptibility (χ_M). Ultralow-temperature (<1.8 K) hysteresis studies and DC relaxation measurements were performed on a single crystal at Grenoble using an array of micro-SQUIDS.[26] The high sensitivity of this magnetometer allows the study of single crystals of SMMs of the order of 10−500 μm. The field can be applied in any direction by separately driving three orthogonal coils. Crystals were maintained in mother liquor to avoid degradation and were covered in grease for protection during the transfer to the micro-SQUID and subsequent cooling.

RESULTS AND DISCUSSION

Synthesis. All the preparations described below were carried out in darkness, in reaction flasks covered with aluminum foil. This was to minimize exposure of the reaction and crystallization solutions to light, which can lead to photodecomposition of $fdcH_2$ in polar media, leading to the release of Fe and the formation of Fe-contaminated products.[13,27] For a similar reason, we also avoided high temperatures.

$[Mn_8O_4(fdc)_6(DMF)_2(H_2O)_2]$ (**1**) was initially isolated as a minor product from the reaction previously developed to prepare $[Mn_{13}O_8(OMe)_6(fdc)_6]$.[15] The reaction of $fdcH_2$ with $[Mn_{12}O_{12}(O_2CMe)_{16}(H_2O)_4]$ in MeOH/MeCN (1:1) produces a brown solution and a lot of brown precipitate, with the Mn_{13} cluster being subsequently isolated from the filtrate. Extraction of the brown solid with DMF and filtration gave a brown filtrate, from which dark brown needles of **1**·4DMF·4H_2O (see Method A, described in the Experimental Section) slowly grew. Unfortunately, the yield of **1** was very low (∼2%), and inspection of the crystals showed the presence of small amounts of an amorphous brown powder. It was easy to separate the crystals from the powder manually, and IR spectra of the latter suggested it to be similar, but not identical to, **1**. Thus, it was clear that this route to **1** was less than satisfactory, and a search for an improved procedure was therefore sought.

An alternative route (Method B, described in the Experimental Section) to higher yields of **1** was developed involving the comproportionation reaction of $Mn(O_2CMe)_2$, $NBu^n_4MnO_4$, and $fdcH_2$ in EtOH/py/NEt_3 (20:1:0.7 v/v). This gave a dark brown solution that soon precipitated a brown powder of **1** in 40% yield. Method B is a comproportionation reaction at a Mn^{II}:Mn^{VII} ratio of 5:2, giving an average Mn oxidation state in the reaction of $Mn^{+3.4}$. This was used to ensure a high oxidation complex, with the EtOH being able to provide reducing equivalents to the solution as required.

Consideration of Methods A and B subsequently allowed an excellent route to these Mn_8 clusters to be developed using a procedure that is a hybrid of the two, i.e., a comproportionation reaction between Mn^{II} and $[Mn_{12}O_{12}(O_2CMe)_{16}(H_2O)_4]$ ($8Mn^{III}$, $4Mn^{IV}$). The latter was considered a milder, possibly cleaner oxidizing agent and oxide source than MnO_4^- for accessing the Mn_8 cluster, requiring only $fdcH_2$ and Mn^{II}, and this was found to be the case. Since the targeted Mn_8 product is $4Mn^{II}4Mn^{III}$, a Mn^{II}:Mn_{12} ratio of ∼20:1 (average ∼$Mn^{+2.5}$) was employed (see eq 1):

$$20Mn^{2+} + Mn^{3+}{}_8Mn^{4+}{}_4 \rightarrow 32Mn^{2.5+} \quad (1)$$

Indeed, the reaction of $Mn(O_2CMe)_2$, $[Mn_{12}O_{12}(O_2CMe)_{16}(H_2O)_4]$, and $fdcH_2$ (20:1:30) in DMF gave a dark brown solution from which $[Mn_8O_4(fdc)_6(DMF)_4]$ (**2**), as **2**·4DMF, was subsequently isolated in an excellent yield of ∼85%, based on Mn. Complex **2** differs from **1** only in the terminal solvent ligands. The formation of Mn_8 from Mn_{12} is obviously a mechanistically very complicated one, so obtaining it in such a high yield from a rational procedure was extremely satisfying. Its preparation is summarized in eq 2,

$$[Mn_{12}O_{12}(O_2CMe)_{16}(H_2O)_4] + 20Mn(O_2CMe)_2 + 24fdcH_2 \rightarrow 4[Mn_8O_4(fdc)_6(DMF)_4] + 56MeCO_2H \quad (2)$$

and it can be seen that this balanced equation corresponds almost exactly to the reaction stoichiometry employed, other than a small (25%) excess of $fdcH_2$, and this is no doubt a major reason for the clean formation of **2** in such an excellent yield.

Description of the Structures. A stereoview of the complete structure of **1** is shown in Figure 1, and the core of the molecule is shown in Figure 2. Selected interatomic distances and angles are listed in Table 2. The molecule lies on a crystallographic C_2-axis along the crystal b-axis and contains a central $[Mn^{III}{}_4(\mu_4\text{-}O)_4]^{4+}$ distorted cubane with each O^{2-} ion also bridging to an external Mn^{II} atom (see Figure 2). The

dx.doi.org/10.1021/ic4011955 | Inorg. Chem. 2013, 52, 10414−10423

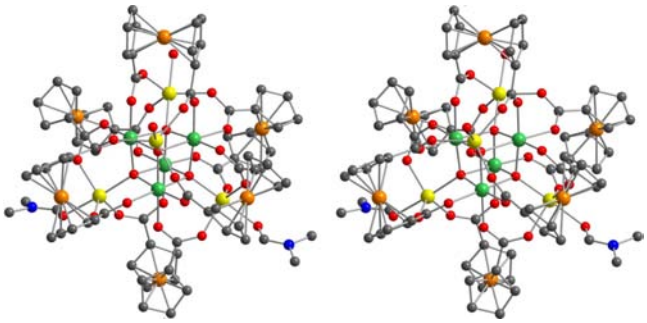

Figure 1. PovRay stereopair of the structure of $[Mn_8O_4(fdc)_6(DMF)_2(H_2O)_2]$ (**1**); H atoms have been omitted for clarity. Color code: light green, Mn^{III}; yellow, Mn^{II}; red, O; orange, Fe; and blue, N.

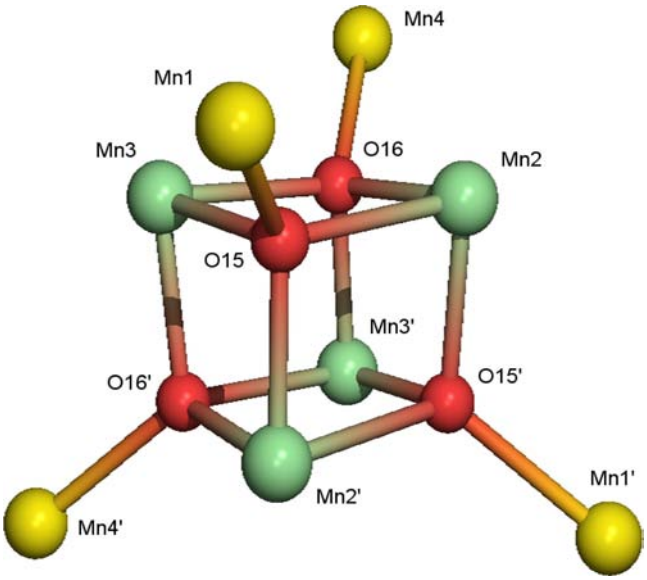

Figure 2. PovRay representation of the $[Mn^{III}_4Mn^{II}_4(\mu_4\text{-}O)_4]^{12+}$ core of **1**. The crystallographic C_2-axis passes through the middle of the Mn2O15Mn2′O15′ face, and the four Mn^{III} JT axes are along the vertical edges of the cubane. Color code: light green, Mn^{III}; yellow, Mn^{II}; and red, O.

resulting $[Mn^{II}_4Mn^{III}_4(\mu_4\text{-}O)_4]^{12+}$ core thus comprises three $4Mn^{III}$, $4Mn^{II}$, and $4O^{2-}$ concentric tetrahedra and has T_d symmetry. This arrangement is not uncommon in the cluster chemistry for other metals[28] and one example was previously found for Mn with pyrazole-based ligands.[29] The peripheral ligation of **1** is completed by six bridging fdc^{2-} groups, two terminal DMF groups, and two terminal H_2O groups. Each carboxylate group of an fdc^{2-} bridges a Mn^{II}/Mn^{III} pair in a *syn*, *syn*, $\eta^1{:}\eta^1{:}\mu_2$-coordination mode. The torsion angles between the two carboxylate groups of each fdc^{2-} vary: four fdc^{2-} groups have torsion angles of <30° (synperiplanar configuration) and the other two have angles between 30° and 90° (synclinal configuration).[30] The overall charge of the molecule is consistent with all ferrocenyl groups being in the reduced form, fdc^{2-}, containing formally Fe^{II}, i.e., none are in the rare oxidized fdc^{-} form containing Fe^{III}, as found for one ligand in $[Fe_7O_3(OMe)(fdc)_6(MeOH)_3]^{3+}$.[13]

The Mn oxidation states were confirmed using bond valence sum (BVS) calculations (see Table 3).[31] The Mn^{III} atoms are near-octahedral, whereas the external Mn^{II} is five-coordinated with a distorted trigonal bipyramidal geometry; the τ parameter

Table 2. Core Interatomic Distances and Angles for Complex 1

interatomic distances (Å)			
Mn1···Mn1′	6.043(8)	Mn3···Mn2′	3.067(2)
Mn1···Mn2	3.448(1)	Mn1−O15	2.074(3)
Mn1···Mn3	3.497(1)	Mn2−O15	1.922(3)
Mn1···Mn4	5.931(3)	Mn2−O16	1.922(2)
Mn1′···Mn4′	3.479(4)	Mn2−O15′	2.220(3)
Mn2···Mn2′	3.115(2)	Mn3−O15	1.930(2)
Mn2···Mn3	2.910(2)	Mn3−O16	1.979(3)
Mn2···Mn3′	3.067(2)	Mn3−O16′	2.138(4)
Mn3···Mn3′	3.092(4)	Mn4−O16	2.065(3)
interatomic angles (°)			
Mn1−O15−Mn2	119.2(1)	Mn3−O16′−Mn2′	98.0(1)
Mn1−O15−Mn3	121.7(1)	Mn3−O16′−Mn3′	97.3(1)
Mn1−O15−Mn2′	119.9(1)	Mn2′-O15′−Mn3′	98.1(1)
Mn2−O15−Mn3	98.1(1)	Mn2′-O16′−Mn3′	96.4(1)
Mn2−O16−Mn3	96.4(1)	Mn4−O16−Mn2	120.2(1)
Mn2−O15′−Mn2′	97.27(9)	Mn4−O16−Mn3	118.7(1)
Mn2−O15′−Mn3′	95.1(1)	Mn4−O16−Mn3′	120.9(1)

Table 3. Bond Valence Sum (BVS) Calculations for 1·4DMF·4H$_2$O

	Bond Valence Sum, BVS[a]		
atom	Mn^{II}	Mn^{III}	Mn^{IV}
Mn1	2.11	1.95	1.91
Mn2	3.28	3.03	2.97
Mn3	3.24	2.99	2.94
Mn4	2.16	1.99	1.96

[a]The underlined value is the closest to the charge for which it was calculated. The oxidation state can be taken as the nearest integer to the underlined value.

is 0.78 and 0.81 for Mn(1) and Mn(4), respectively, where τ = 0 for ideal sp geometries and τ = 1 for ideal tbp geometries.[32] The four Mn^{III} are Jahn−Teller (JT)-distorted, with axial elongations of 0.265 and 0.451 Å for Mn3 and Mn2, respectively, compared with the average bond lengths in the equatorial plane. The four JT axes are O9−Mn3−O16′ and O12−Mn2−O15′, and they are arranged nearly parallel. Thus, they elongate four parallel edges of the central cubane (Figure 2). The compound has crystallographic C_2 symmetry, but virtual D_2 symmetry (if the DMF vs H_2O difference in terminal ligands is ignored).

The core of complex **2** is shown in Figure 3, and selected interatomic distances and angles are listed in Table 4. Complex **2** is essentially isostructural with **1**, except for the presence of four DMF ligands instead of the two DMF and two water ligands in **1**. The binding modes of the fdc^{2-} groups are as described for **1**. The molecule lies in a general position and thus has crystallographic C_1 symmetry but again virtual D_2 symmetry. Similarly, the Mn oxidation states were confirmed by BVS calculations (Table 5) and, as in the case of **1**, all the Jahn−Teller elongation axes are essentially parallel. Thus, in both **1** and **2**, the two cubane faces perpendicular to the elongation direction are essentially squares (more accurately, essentially rhombuses), whereas the remaining four faces in each complex are essentially rectangles (rhomboids), as shown in Figure 4.

Structural Differences between 1 and 2. Although the overall structures of **1** and **2** are very similar, as described

dx.doi.org/10.1021/ic4011955 | *Inorg. Chem.* 2013, 52, 10414−10423

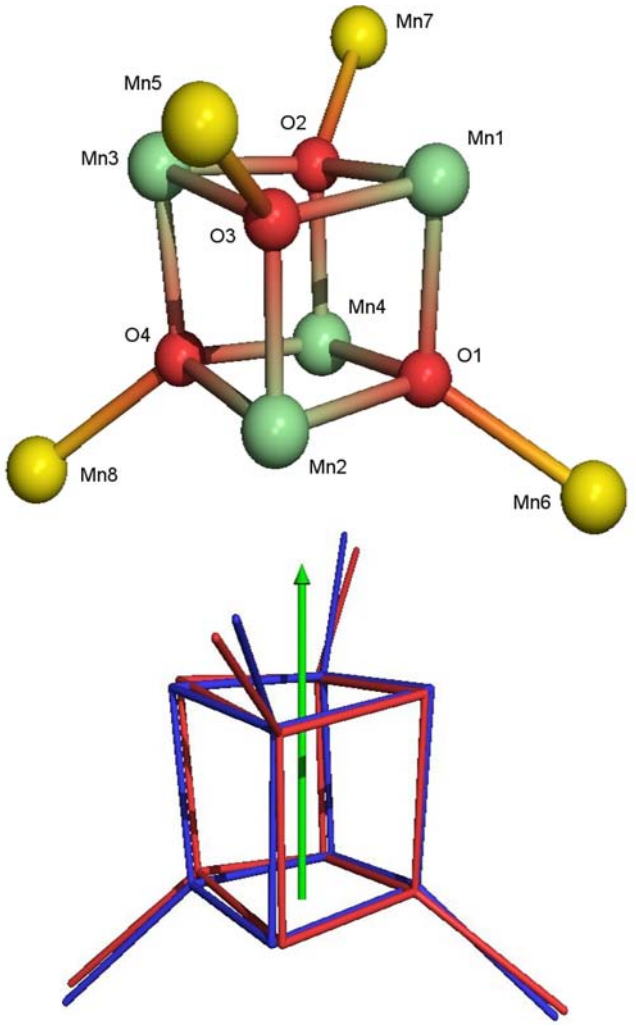

Figure 3. (Top) Pov-Ray representation of the $[Mn^{III}_4Mn_4^{II}(\mu_4\text{-}O)_4]^{12+}$ core of **2** (color code: light green, Mn^{III}; yellow, Mn^{II}; and red, O). (Bottom) Overlap of the cores **1** (blue) and **2** (red). The green arrow indicates the direction of the Jahn–Teller elongations.

above, closer comparison of their $[Mn^{II}_4Mn^{III}_4(\mu_4\text{-}O)_4]^{12+}$ cores shows some slight but significant differences in both interatomic distances and angles. This is reflected in Figure 3 (bottom), which shows that the cores are almost but not quite superimposable, with noticeable differences particularly in some angles within the central cubane and those to the external Mn^{II} atoms. Even small differences in bridging angles can significantly affect the exchange interactions between two metal atoms, and the small but significant difference in core metric parameters is believed to be the origin of the different magnetic properties of **1** and **2** (vide infra).

More specifically, the JT elongations for **2** are noticeably longer than those in **1**, particularly within the cubane (see Table 6). The average elongated Mn^{III}–O^{2-} bonds are 2.179 and 2.303 Å for **1** and **2**, respectively, while the nonelongated Mn^{III}–O^{2-} bonds in the cubane are, correspondingly, 1.938 and 1.890 Å. The central cubane in **2** is thus more elongated and has a smaller cross-section than in **1**. Probably as a result of this, the Mn^{II}–O–Mn^{III} angles are slightly smaller in **2** vs **1** (average 120.4° vs 119.4°). Another peculiarity of **2** is found in the Mn^{II} geometries: for Mn6 and Mn7, the τ values are 0.84 and 0.74, respectively, indicating distorted tbp geometry as in **1**, but those at Mn5 and Mn8 are 0.22 and 0.54, respectively, indicating distorted sp and intermediate geometries, respectively. All these differences are also reflected in small but real changes of a few degrees to the fdc^{2-} torsion angles, as the latter adjust to accommodate the differing distortions and coordination geometries. We have no reason to assume that the differences between **1** and **2** are due to anything other than differing packing forces in the different crystal space groups, but they nevertheless are expected to be (and are) reflected in the magnetic properties of the complexes. Note that the packing will be dominated by the large Mn_8 molecules, so changes to the lattice solvent content of the solids upon vacuum drying are reasonably assumed to have minimal effect on the structures of the Mn_8 molecules. Finally, both complexes show no significant intermolecular contacts, other than the expected weak C–H···π and C–H···O contacts (see Figure S1 in the Supporting Information),[33] and we consequently do not anticipate noticeable intermolecular exchange interactions.

Table 4. Core Interatomic Distances and Angles for Complex 2

interatomic distances (Å)			
Mn1···Mn2	3.205(5)	Mn1–O2	1.895(4)
Mn1···Mn3	2.831(5)	Mn1–O3	1.885(2)
Mn1···Mn4	3.114(5)	Mn2–O1	1.904(2)
Mn1···Mn5	3.384(1)	Mn2–O3	2.340(7)
Mn1···Mn6	3.730(7)	Mn2–O4	1.884(3)
Mn1···Mn7	3.476(3)	Mn3–O2	1.903(2)
Mn1···Mn8	5.617(2)	Mn3–O3	1.872(4)
Mn2···Mn3	3.128(3)	Mn3–O4	2.310(7)
Mn2···Mn4	3.149(5)	Mn4–O1	1.885(3)
Mn3···Mn4	3.149(5)	Mn4–O2	2.267(7)
Mn1–O1	2.295(7)	Mn4–O4	1.892(2)
interatomic angles (°)			
Mn1–O1–Mn2	99.12(8)	Mn5–O3–Mn1	117.41(9)
Mn1–O3–Mn2	98.10(8)	Mn5–O3–Mn2	119.12(9)
Mn1–O2–Mn3	96.39(9)	Mn5–O3–Mn3	123.8(1)
Mn1–O3–Mn3	97.78(9)	Mn6–O1–Mn1	117.12(9)
Mn1–O1–Mn4	95.83(8)	Mn6–O1–Mn2	119.8(1)
Mn1–O2–Mn4	96.50(8)	Mn6–O1–Mn4	123.0(1)
Mn2–O3–Mn3	95.24(8)	Mn7–O2–Mn1	122.7(1)
Mn2–O4–Mn3	95.93(8)	Mn7–O2–Mn3	117.31(9)
Mn2–O1–Mn4	96.77(8)	Mn7–O2–Mn4	120.68(9)
Mn2–O4–Mn4	97.23(8)	Mn8–O4–Mn2	123.2(1)
Mn3–O2–Mn4	97.71(8)	Mn8–O4–Mn3	120.82(9)
Mn3–O4–Mn4	96.59(8)	Mn8–O4–Mn4	117.3 (1)

Table 5. Bond Valence Sum (BVS) Calculations for 2•4DMF

	Bond Valence Sum, BVS[a]		
atom	Mn^{II}	Mn^{III}	Mn^{IV}
Mn1	3.34	<u>3.08</u>	3.03
Mn2	3.34	<u>3.08</u>	3.02
Mn3	3.43	<u>3.17</u>	3.11
Mn4	3.41	<u>3.14</u>	3.08
Mn5	<u>2.09</u>	1.92	1.89
Mn6	<u>2.10</u>	1.93	1.90
Mn7	<u>2.08</u>	1.92	1.88
Mn8	<u>2.09</u>	1.92	1.89

[a]The underlined value is the closest to the charge for which it was calculated. The oxidation state can be taken as the nearest integer to the underlined value.

dx.doi.org/10.1021/ic4011955 | *Inorg. Chem.* 2013, 52, 10414–10423

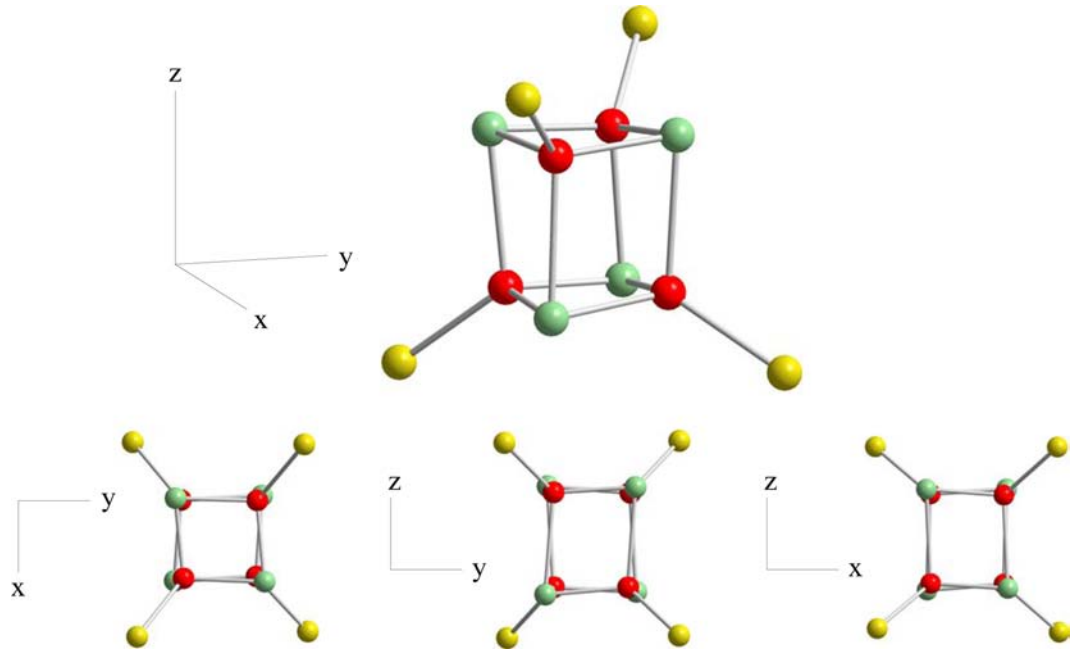

Figure 4. Orthogonal views of the cubane core of **2**, emphasizing the elongation along the *z*-direction caused by the Mn^{III} JT distortions. The core of **1** is very similar.

Table 6. Bond Distances and Angles Involving JT Elongated Bonds in 1 and 2

parameter[a]	1	2
Mn^{III}–O_c[b]	2.138(4) Å	2.340(7) Å, 2.267(7)
	2.220(3) Å	2.310(7) Å, 2.295(7)
average	2.179 Å	2.303 Å
Mn^{III}–O_f[b]	2.083(4) Å	2.149(7) Å, 2.167(7)
	2.136(3) Å	2.149(7) Å, 2.145(7)
average	2.110 Å	2.153 Å
$O_c\cdots O_f$ (av)[c]	4.289 Å	4.456 Å
Mn^{III}–O_c (av)[d]	1.938 Å	1.890 Å
difference, Δ[e]	0.241 Å	0.413 Å
Mn^{II}–O–Mn^{III}[f]	119.9(1)°	119.12(9)°, 120.68(9)°
	120.9(1)°	117.12(9)°, 120.82(9)°
average	120.4°	119.44°

[a]Index legend: c = cubane, f = fdc^{2-} carboxylate. [b]JT elongated bonds. [c]Sum of the two JT elongated bonds. [d]Nonelongated bonds. [e]Difference between JT elongated and nonelongated averages. [f]Angle including the JT elongated Mn^{III}–O_c bond.

Magnetochemistry. Variable-temperature, DC magnetic susceptibility data were collected on powdered microcrystalline samples of vacuum-dried **1**·3DMF and **2**·$^3/_2$DMF·$3H_2O$, restrained in eicosane to prevent torquing, in the 5.0–300.0 K range with an applied field of 1000 Oe (0.1 T). The obtained data are plotted as $\chi_M T$ vs T in Figure 5.

The value of $\chi_M T$ for **1**·3DMF does not change much with temperature, decreasing from 16.52 cm^3 K mol^{-1} at 300 K to a minimum of 14.71 cm^3 K mol^{-1} at 150 K, then slightly increasing to a maximum of 15.56 cm^3 K mol^{-1} at 35 K, and then finally decreasing to 13.64 cm^3 K mol^{-1} at 5.00 K. The 300 K value, which is much less than that for a $Mn^{II}_4Mn^{III}_4$ system

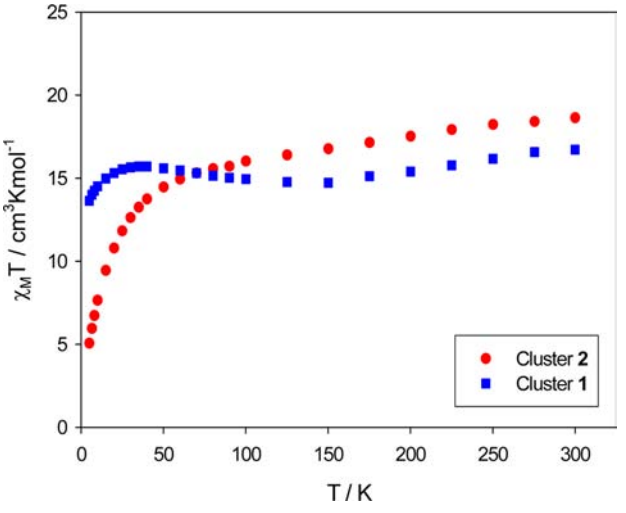

Figure 5. $\chi_M T$ vs T plots for **1**·3DMF and **2**·$^3/_2$DMF·$2H_2O$ in a 0.1 T DC field.

of noninteracting ions (29.5 cm^3 K mol^{-1}), and the overall plot profile indicate predominantly antiferromagnetic interactions among the Mn ions and a significant ground-state spin, S. The 5.00 K value suggests an $S = 5$ ground state with $g < 2$ (spin-only ($g = 2$) value for $S = 5$ is 15 cm^3 K mol^{-1}). For **2**·$^3/_2$DMF·$3H_2O$, $\chi_M T$ at 300 K is 18.64 cm^3 K mol^{-1}, and it decreases slowly with temperature down to ~80 K, and then decreases more rapidly, reaching 4.99 cm^3 K mol^{-1} at 5.00 K. The steeply decreasing plot at the lowest temperatures makes it difficult to estimate the ground state, but it appears to be in the $S = 0$–3 range, which is significantly different from **1**·3DMF.

The nuclearity and complexity of the structure of **1** and **2** prevent application of the Kambe vector coupling method[34] to determine the pairwise Mn_2 exchange coupling constants (J_{ij}). We concentrated, instead, on identifying the ground-state S values from variable-temperature (T) and variable-field (H) DC magnetization (M) data, and AC susceptibility data. Magnet-

dx.doi.org/10.1021/ic4011955 | Inorg. Chem. 2013, 52, 10414–10423

ization data were acquired in the 1.8−10.0 K and 0.1−7 T ranges, and fit by diagonalization of the spin Hamiltonian matrix using the MAGNET program,[24] which assumes that only the ground state is populated, includes axial zero-field splitting ($D\hat{S}_z^2$) and the Zeeman interaction, and incorporates a full powder average. The corresponding spin Hamiltonian is given by eq 3:

$$\mathcal{H} = D\hat{S}_z^2 + g\mu_B\mu_0\hat{S}H \quad (3)$$

where $\hat{S}_z$ is the easy-axis spin operator, μ_B is the Bohr magneton, and μ_0 is the vacuum permeability.

For **1**·3DMF, a satisfactory fit could only be obtained if data collected at fields above 4T were excluded. This suggested the presence of low-lying excited states, as expected for a high nuclearity complex containing multiple Mn^{II} ions, and that some of these have greater spin than the ground state and are being stabilized by the applied field causing them to be significantly populated. The data are plotted in Figure 6 as

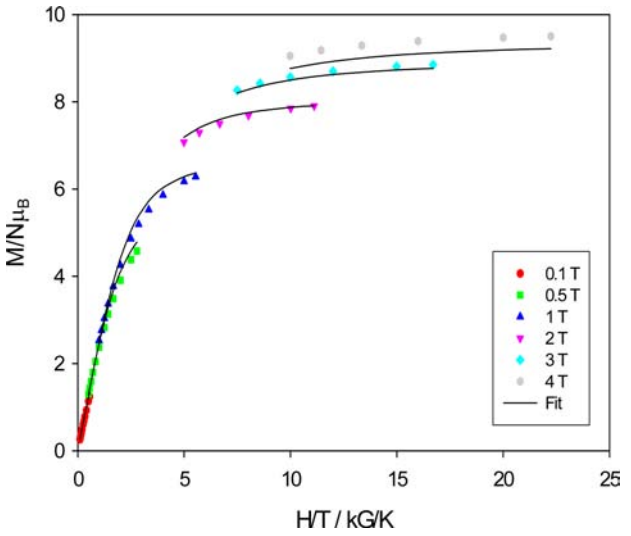

Figure 6. Plot of reduced magnetization ($M/N\mu_B$) vs H/T for **1**·3DMF for data collected at the indicated fields. The solid lines are the fit of the data. See text for the fit parameters.

reduced magnetization ($M/N\mu_B$) vs H/T, and the fit (solid lines) gave $S = 5$, $g = 1.97(2)$, and $D = -0.32(4)$ cm^{-1}. Alternative fits with $S = 4$ or 6 were rejected, because of their unreasonable g-values. The g vs D root-mean-square error surface of the fit was obtained with the GRID program[35] and is shown as a 2-D contour plot in Figure S2 in the Supporting Information;[33] this allowed the indicated fit uncertainties to be estimated. Figure S2 in the Supporting Information also indicates an alternative fit with $D > 0$, but it is clearly of much poorer quality. For **2**·$^3/_2$DMF·$2H_2O$, we could not get a satisfactory fit, even just using data collected at low fields, suggesting particularly low-lying excited states with higher spin than the ground state.

As an alternative means of probing the ground states of **1**·3DMF and **2**·$^3/_2$DMF·$2H_2O$ in the absence of complications from a DC field, AC susceptibility data were collected in the 1.8−15.0 K range in a 3.5 G AC field oscillating at 50, 250, and 997 Hz. The in-phase AC susceptibility (χ'_M) of **1**·3DMF is plotted as χ'_MT vs T in the top panel of Figure 7. It exhibits a monotonic decrease with decreasing temperature, which is consistent with depopulation of excited states of higher spin

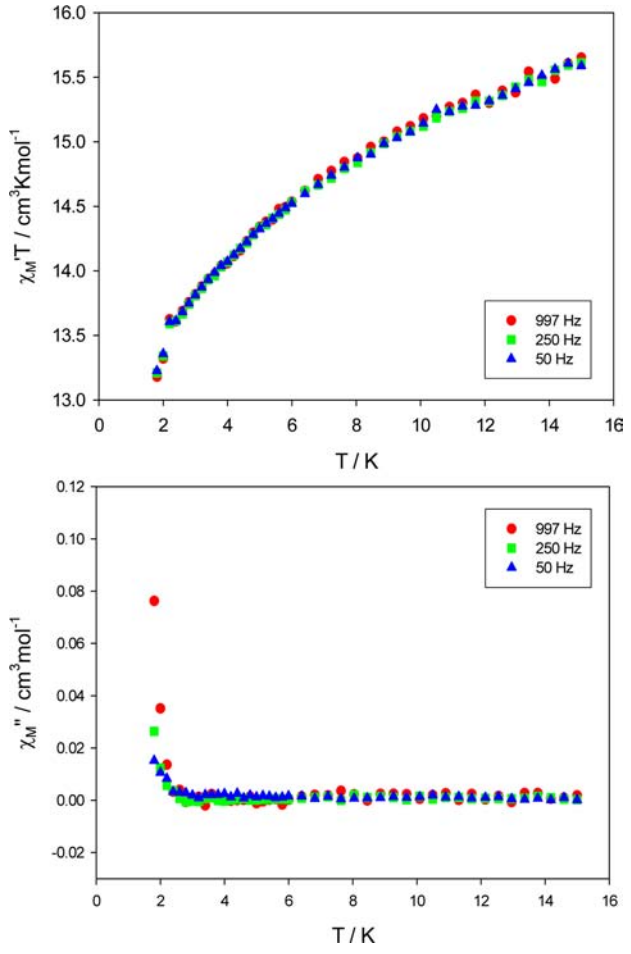

Figure 7. AC in-phase χ'_MT vs T plots (top panel) and out-of-phase χ''_M vs T plots (bottom panel) for **1**·3DMF in the 1.8−15 K range.

than the ground state, supporting the conclusion of the DC magnetization fit. To determine the ground state, the plot is extrapolated to 0 K from a point that avoids the typical accelerated decrease at the lowest temperatures from slow relaxation of an SMM and/or weak intermolecular interactions, ZFS, etc. Extrapolation from above ~6 K gives a χ'_MT value in the range of 13.5−14.0 cm^3 K mol^{-1}, which is consistent with $S = 5$ and $g = 1.90-1.93$; $S = 4$ and 6 should give values of slightly less than 10 and 21 cm^3 K mol^{-1}, respectively, which are very different from the experimental value. The AC data thus support the DC data in indicating an $S = 5$ ground state for **1**·3DMF.

The out-of-phase AC susceptibility χ''_M vs T plot below 3 K in the bottom panel of Figure 7 shows weak tails from signals whose peak maxima lie below 1.8 K, suggesting the slow relaxation of a SMM. This was explored further by DC studies down to 0.04 K on single crystals of **1**·4DMF·$4H_2O$ maintained in mother liquor until measurement. The resulting magnetization vs applied DC field scans (Figure 8) exhibit hysteresis loops whose coercivities increase with decreasing T, as expected for a SMM. The loops are rather unremarkable, showing no well-defined quantum tunneling of magnetization (QTM) steps except a very broad one at zero field. This broadness is undoubtedly due to a combination of the low-lying excited states, weak intermolecular interactions, and the disorder seen in the crystal structure, all of which will serve to broaden and smear out the steps.

dx.doi.org/10.1021/ic4011955 | Inorg. Chem. 2013, 52, 10414−10423

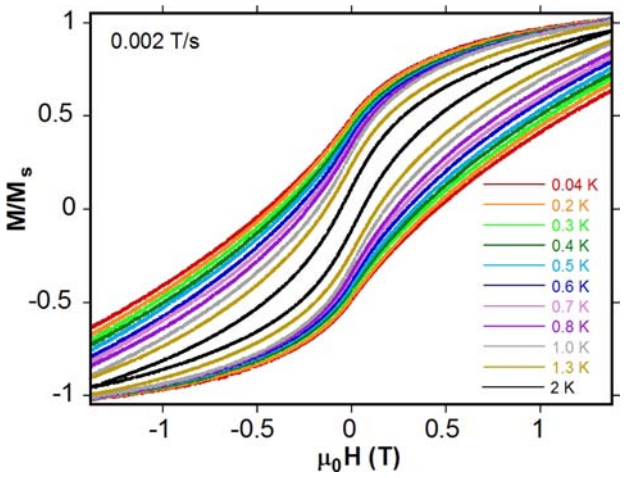

Figure 8. Magnetization versus DC field scans for a single crystal of **1**·4DMF·4H_2O at the indicated temperatures and a scan rate of 0.002 T/s. The magnetization is normalized to its maximum value, M_S.

The in-phase χ'_MT vs T plot for **2**·$^3/_2$DMF·3H_2O in the top panel of Figure 9 is distinctly different from that for **1**·3DMF, in agreement with the differences of Figure 5. It decreases from

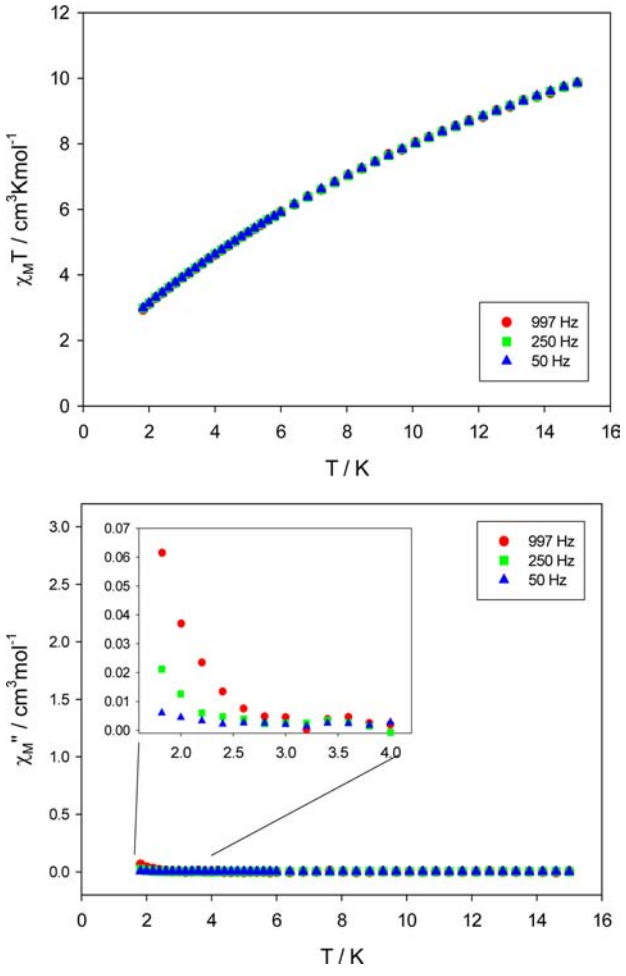

Figure 9. AC in-phase χ'_MT vs T plot (top panel) and out-of-phase χ''_M vs T plots (bottom panel) for **2**·$^3/_2$DMF·2H_2O in the 1.8−15 K range. The inset shows an expanded view, emphasizing the weak, frequency-dependent χ''_M tails.

9.86 cm^3 K mol^{-1} at 15 K to 2.98 cm^3 K mol^{-1} at 1.8 K. This large decrease over a small T range supports the conclusion, from the DC data, that there are particularly low-lying excited states with spin greater than that of the ground state. This makes data extrapolation more difficult, but with the same assumptions as for **1**·3DMF, it gives a value of ∼2.5−3.0 cm^3 K mol^{-1}, indicating a ground state of S = 2. Expected values for S = 1 and 3 are 1.0 and 6.0 cm^3 K mol^{-1}, respectively, for g = 2.0, which are distinctly different from the experimental data. The out-of-phase AC susceptibility χ''_M vs T plot in the bottom panel of Figure 9 again shows weak, frequency-dependent tails, indicating that **2**·$^3/_2$DMF·2H_2O also might possibly be an SMM. However, this was not explored further with micro-SQUID studies, given the broad hysteresis loops for **1**·4DMF·4H_2O and the greater density of low-lying excited states in **2**.

Electrochemical measurements were attempted on both clusters **1** and **2**. Although they are very slightly soluble in neat DMF, they were found to be essentially completely insoluble in DMF that contained a large excess of supporting electrolyte, and we could not record an adequate signal. For the same reasons, we were unable to record UV−vis spectra in solution.

Origin of the Different Spin Ground States. The structures of **1** and **2** are identical to first order, differing only in the solvent ligands; however, closer inspection shows small but statistically real differences in core metric parameters, almost certainly due to different packing forces. These small structural differences are very likely the cause of the significant differences in magnetic properties, with the two complexes having different ground states of S = 5 and 2, respectively. This can be rationalized as a combination of spin frustration effects from competing exchange interactions and the presence of many exchange interactions involving Mn^{II} atoms, which are expected to be very weak. Under virtual D_2 symmetry, there will be four sets of exchange interactions (J), two $Mn^{II}\cdots Mn^{III}$ and two $Mn^{III}\cdots Mn^{III}$; the long-range $Mn^{II}\cdots Mn^{II}$ are assumed to be zero. The four parallel Mn^{III} JT elongation axes will align the four Mn d_{z^2} magnetic orbitals parallel, very likely leading to both antiferro- and ferromagnetic interactions in the central cubane: (i) the former are predicted for the Mn2Mn3 and Mn2′Mn3′ pairs (Figure 2), as seen for other Mn^{III}_2 interactions when the two JT axes are perpendicular to the $\{Mn_2(\mu\text{-}O^{2-})_2\}$ plane;[36] and (ii) the latter are predicted for the four remaining Mn_2 pairs in Figure 2, where σ overlap of d_{z^2} orbitals with empty $d_{x^2-y^2}$ will provide a major ferromagnetic coupling pathway, as again seen in other Mn^{III}_x clusters containing ferromagnetic Mn^{III}_2 pairs with this orbital arrangement.[5,37] Since the Mn_8 core can be considered the fusion of Mn_3 trangular units, there will be extensive spin frustration effects, defined here in the way preferred by the chemistry community, i.e., competing exchange interactions (J_{ij}) of comparable magnitude that frustrate the preferred spin alignments and lead, instead, to intermediate alignments. As a result, the ground state becomes very sensitive to the relative magnitude of the competing interactions. Since most, if not all, of the interactions in **1** and **2** are expected to be relatively weak, the presence of low-lying excited states is not surprising, and neither is the observation that even small structural differences can thus sufficiently affect the constituent J values and their relative ratio to give a change in the ground state. This is well with precedent: for example, certain Mn_7 clusters with either S = 11 or 16 ground states, depending on small structural differences,[38] which we identified as affecting the relative ratio of the two weakest J couplings in the molecules. In this

dx.doi.org/10.1021/ic4011955 | Inorg. Chem. 2013, 52, 10414−10423

previous work, we determined the constituent J values from DFT calculations, allowing us to identify the spin alignments leading to $S = 11$ or 16 ground states in the two cases. We have not pursued such a full analysis in the present studies on **1** and **2**; however, the following qualitative rationalization can nevertheless be offered. If the ferromagnetic $Mn^{III}\cdots Mn^{III}$ interactions of the central cube dominate the antiferromagnetic $Mn^{III}\cdots Mn^{III}$ ones, then the central Mn^{III} spins will all align parallel, and the expected antiferromagnetic $Mn^{II}\cdots Mn^{III}$ interactions will then give an $S = 10 - 8 = 2$ ground state, as seen experimentally for **2**. If the central ferromagnetic $Mn^{III}\cdots Mn^{III}$ interactions do not dominate, then intermediate spin alignments will result, the spin of the cubane will be decreased (compared to that in **2**), and the molecular spin will thus be increased, consistent with the $S = 5$ ground state observed for **1**.

CONCLUSIONS

The use of 1,1′-ferrocenedicarboxylic acid in Mn cluster chemistry has resulted in a mixed-valence Mn_8 oxide-bridged complex with only fdc^{2-} peripheral ligation (other than bound solvent molecules). The high isolated yield (85%) of complex **2** from a comproportionation reaction is particularly noteworthy: such high yields are very unusual in polynuclear cluster chemistry, especially with fdc^{2-} ligation, and extensions to this synthetic approach are being explored. The magnetic differences between **1** and **2** provide another example of how small structural changes to a spin-frustrated system can significantly affect the ground state through small changes to the relative magnitudes of competing interactions. We had hoped to also study these Mn_8 clusters in solution, where we expect them to behave identically as packing forces are relaxed and the structures become identical; however, we have found both **1** and **2** to be extremely insoluble in all tested solvents, which unfortunately is the typical behavior of neutral fdc^{2-} ligated clusters. This has also frustrated attempts to characterize the multiredox properties of this cluster via electrochemistry, which was one of the original objectives of this work. Nevertheless, with large amounts finally available, it opens up the field for further studies of the reactivity of these species.

ASSOCIATED CONTENT

Supporting Information

X-ray crystallographic files in CIF format for complex **1**·4DMF·$4H_2O$ and **2**·4DMF. This material is available free of charge via the Internet at http://pubs.acs.org.

AUTHOR INFORMATION

Corresponding Author

*Tel.: +1-352-392-8314. Fax: +1-352-392-8757. E-mail address: christou@chem.ufl.edu.

Notes

The authors declare no competing financial interest.

ACKNOWLEDGMENTS

We thank the National Science Foundation (Grant Nos. CHE-0910472 and DMR-1213030) and the ERC Advanced Grant MolNanoSpin (No. 226558) for support of this work.

REFERENCES

(1) (a) Bagai, R.; Christou, G. *Chem. Soc. Rev.* **2009**, *38*, 1011. (b) Aromi, G.; Brechin, E. K. *Struct. Bonding (Berlin)* **2006**, *122*, 1.

(2) (a) Christou, G.; Gatteschi, D.; Hendrickson, D. N.; Sessoli, R. *MRS Bull.* **2000**, *25*, 66. (b) Tasiopoulos, A. J.; Perlepes, S. P. *Dalton Trans.* **2008**, *41*, 5537. (c) Glaser, T. *Chem. Commun.* **2011**, *47*, 116. (d) Aromi, G.; Aubin, S. M. J.; Bolcar, M. A.; Christou, G.; Eppley, H. J.; Folting, K.; Hendrickson, D. N.; Huffman, J. C.; Squire, R. C.; Tsai, H.-L.; Wang, S.; Wemple, M. W. *Polyhedron* **1998**, *17*, 3005.

(3) Boudalis, A. K.; Sanakis, Y.; Raptopoulou, C. P.; Psycharis, V. In *Magnetism and Superconductivity in Low-Dimensional Solids*; Stamopoulos, D., Ed.: Nova Science: New York, 2008.

(4) Gatteschi, D.; Sessoli, R.; Villain, J. *Molecular Nanomagnets*; Oxford University Press: New York, 2006.

(5) Roubeau, O.; Clérac, R. *Eur. J. Inorg. Chem.* **2008**, 4325.

(6) (a) Katoh, K.; Isshiki, H.; Komeda, T.; Yamashita, M. *Coord. Chem. Rev.* **2011**, *255*, 2124. (b) Woodruff, D. N.; Winpenny, R. E. P.; Layfield, R. A. *Chem. Rev.* **2013**, *113*, 5110.

(7) (a) Osa, S.; Kido, T.; Matsumoto, N.; Re, N.; Pochaba, A.; Mrozinski, J. *J. Am. Chem. Soc.* **2004**, *126*, 420. (b) Liu, J.-L.; Guo, F.-S.; Meng, Z.-S.; Zheng, Y.-Z.; Leng, J.-D.; Tong, M.-L.; Ungur, L.; Chibotaru, L. F.; Heroux, K. J.; Hendrickson, D. N. *Chem. Sci.* **2011**, *2*, 1268. (c) Papatriantafyllopoulou, C.; Wernsdorfer, W.; Abboud, K. A.; Christou, G. *Inorg. Chem.* **2011**, *50*, 421. (d) Holinska, M.; Premuzic, D.; Jeon, I.-R.; Wernsdorfer, W.; Clérac, R.; Dehnen, S. *Chem.—Eur. J.* **2011**, *17*, 9605. (e) Stamatatos, T. C.; Teat, S. J.; Wernsdorfer, W.; Christou, G. *Angew. Chem., Int. Ed.* **2009**, *48*, 521. (f) Mereacre, V.; Ako, A. M.; Clerac, R.; Wernsdorfer, W.; Filoti, G.; Bartolome, J.; Anson, C. E.; Powell, A. K. *J. Am. Chem. Soc.* **2007**, *129*, 9248. (g) Mereacre, V.; Ako, A. M.; Clerac, R.; Wernsdorfer, W.; Hewitt, I. J.; Anson, C. E.; Powell, A. K. *Chem.—Eur. J.* **2008**, *14*, 3577. (h) Langley, S.; Moubaraki, B.; Murray, K. S. *Dalton Trans.* **2010**, *39*, 5066. (i) Saha, A.; Thompson, M.; Abboud, K. A.; Wernsdorfer, W.; Christou, G. *Inorg. Chem.* **2011**, *50*, 10476.

(8) Stamatatos, T. C.; Christou, G. *Inorg. Chem.* **2009**, *48*, 3308.

(9) (a) Meng, X.; Hou, H.; Li, G.; Ye, B.; Ge, T.; Fan, Y.; Zhu, Y.; Sakiyama, H. *J. Organomet. Chem.* **2004**, *689*, 1218. (b) Lee, S.-M.; Cheung, K.-K.; Wong, W.-T. *J. Organomet. Chem.* **1996**, *506*, 77. (c) Cotton, F. A.; Daniels, L. M.; Lin, C.; Murillo, C. A. *J. Am. Chem. Soc.* **1999**, *121*, 4538. (d) Uhl, W.; Spies, T.; Haase, D.; Winter, R.; Kaim, W. *Organometallics* **2000**, *19*, 1128. (e) Dong, G.; Li, Y.-t.; Duan, C.-y.; Hong, M.; Meng, Q.-j. *Inorg. Chem.* **2003**, *42*, 2519.

(10) (a) Meng, X.; Cheng, W.; Mi, L.; Tang, M.; Hou, H. *Inorg. Chem. Commun.* **2006**, *9*, 662. (b) Das, N.; Arif, A. M.; Stang, P. J.; Sieger, M.; Sarkar, B.; Kaim, W.; Fiedler, J. *Inorg. Chem.* **2005**, *44*, 5798. (c) Guo, D.; Zhang, B.-G.; Duan, C.-y.; Cao, X.; Meng, Q.-J. *Dalton Trans.* **2003**, 282. (d) Zheng, G.-L.; Ma, J.-F.; Su, Z.-M.; Yan, L.-K.; Yang, J.; Li, Y.-Y.; Liu, J.-F. *Angew. Chem., Int. Ed.* **2004**, *43*, 2409. (e) Chandrasekhar, V.; Thirumoorthi, R. *Organometallics* **2007**, *26*, 5415. (f) Kim, Y. S.; Kim, J.; Kim, D.; Chae, H. K. *Chem. Lett.* **2007**, *36*, 150. (g) Meng, X.; Li, G.; Hou, H.; Han, H.; Fan, Y.; Zhu, Y.; Du, C. *J. Organomet. Chem.* **2003**, *679*, 153. (h) Mereacre, V.; Prodius, D.; Ako, A. M.; Shova, S.; Turta, C.; Wurst, K.; Jaitner, P.; Powell, A. K. *Polyhedron* **2009**, *28*, 3551.

(11) (a) Wang, L.; Meng, X.; Zhang, E.; Hou, H.; Fan, Y. *J. Organomet. Chem.* **2007**, *692*, 4367. (b) Bera, J. K.; Clerac, R.; Fanwick, P. E.; Walton, R. A. *J. Chem. Soc., Dalton Trans.* **2002**, 2168. (c) Maksakov, V. A.; Slovohotova, I. V.; Golovin, A. V.; Babailov, S. P. *Russ. Chem. Bull.* **2001**, *50*, 2451. (d) Cowley, A. R.; Hector, A. L.; Hill, A. F.; White, A. J. P.; Williams, D. J.; Wilton-Ely, J. D. E. T. *Organometallics* **2007**, *26*, 6114. (e) Kuehnert, J.; Rueffer, T.; Ecorchard, P.; Braeuer, B.; Lan, Y.; Powell, A. K.; Lang, H. *Dalton Trans.* **2009**, 4499. (f) Lu, E.-N.; Zhang, J.; Zhu, L.-M.; Xu, Y.; Fan, Y.-T. *Wuji Huaxue Xuebao* **2008**, *24*, 201.

(12) (a) Wen, L.-L.; Zhang, B.-G.; Peng, Z.-H.; Ren, J.-G.; Cai, P.; Duan, C.-Y. *Wuji Huaxue Xuebao* **2004**, *20*, 1228. (b) Yang, Y.-Y.; Wong, W.-T. *Chem. Commun.* **2002**, 2716. (c) Boyd, D. A.; Fanwick, P. E.; Ren, T. *Inorg. Chim. Acta* **2011**, *370*, 198. (d) Tanaka, S.; Yagyu, A.; Kikugawa, M.; Ohashi, M.; Yamagata, T.; Mashima, K. *Chemistry* **2011**, *17*, 3693. (e) Fandos, R.; Hernandez, C.; Otero, A.; Rodriguez, A.; Ruiz, M. J.; Suizo, S.; Pastor, C.; Terreros, P. *Inorg. Chim. Acta*

2011, *366*, 122. (f) Kwag, J. S.; Jeong, M. H.; Lough, A. J.; Kim, J. C. *Bull. Korean Chem. Soc.* **2010**, *31*, 2069.
(13) Masello, A.; Sanakis, Y.; Boudalis, A. K.; Abboud, K. A.; Christou, G. *Inorg. Chem.* **2011**, *50*, 5646.
(14) Gerbier, P.; Ruiz-Molina, D.; Domingo, N.; Amabilino, D. B.; Vidal-Gancedo, J.; Tejada, J.; Hendrickson, D. N.; Veciana, J. *Monatsh. Chem.* **2003**, *134*, 265.
(15) Masello, A.; Murugesu, M.; Abboud, K. A.; Christou, G. *Polyhedron* **2007**, *26*, 2276.
(16) Kondo, M.; Shinagawa, R.; Miyazawa, M.; Kabir, M. K.; Irie, Y.; Horiba, T.; Naito, T.; Maeda, K.; Utsuno, S.; Uchida, F. *Dalton Trans.* **2003**, 515.
(17) Mereacre, V.; Ako, A. M.; Filoti, G.; Bartolome, J.; Anson, C. E.; Powell, A. K. *Polyhedron* **2010**, *29*, 244.
(18) Jankolovits, J.; Kampf, J. W.; Maldonado, S.; Pecoraro, V. L. *Chem.—Eur. J.* **2010**, *16*, 6786.
(19) Diaconescu, P. *Comments Inorg. Chem.* **2010**, *31*, 196.
(20) (a) Lis, T. *Acta Crystallogr., Sect. B: Struct. Sci.* **1980**, *36*, 2042. (b) Sessoli, R.; Tsai, H.-L.; Schake, A. R.; Wang, S.; Vincent, J. B.; Folting, K.; Gatteschi, D.; Christou, G.; Hendrickson, D. N. *J. Am. Chem. Soc.* **1993**, *115*, 1804.
(21) Sheldrick, G. M. *Acta Crystallogr., Sect. A: Found. Crystallogr.* **2008**, *A64*, 112.
(22) *SAINT*. Bruker AXS, Inc.: Madison, WI, USA, 2007.
(23) Spek, A. L. *J. Appl. Crystallogr.* **2003**, *36*, 7.
(24) Davidson, E. R. *MAGNET*, Indiana University: Bloomington, IN, 1999.
(25) Weast, R. C. *CRC Handbook of Chemistry and Physics*; CRC Press: Boca Raton, FL, 1984.
(26) Wernsdorfer, W. *Adv. Chem. Phys.* **2001**, *118*, 99.
(27) (a) Ali, L. H.; Cox, A.; Kemp, T. J. *Chem. Commun.* **1972**, 265. (b) Bozak, R. E. *Adv. Photochem.* **1971**, *8*, 227. (c) Ali, L. H.; Cox, A.; Kemp, T. J. *Dalton Trans.* **1973**, 1468. (d) Nesmeyanov, A. N.; Sazonova, V. A.; Romanenko, V. I.; Zol'nikova, G. P. *Izv. Akad. Nauk SSSR, Ser. Khim.* **1965**, 1694.
(28) (a) Liu, L.; Zakharov, L. N.; Rheingold, A. L.; Hanna, T. A. *Chem. Commun.* **2004**, *13*, 1472. (b) Raptis, R. G.; Georgakaki, I. P.; Hockless, D. C. R. *Angew. Chem., Int. Ed.* **1999**, *38*, 1632. (c) Chakraborty, I.; Baran, P.; Sanakis, Y.; Simopoulos, A.; Fachini, E.; Raptis, R. G. *Inorg. Chem.* **2008**, *47*, 11734. (d) Gass, I. A.; Milios, C. J.; Whittaker, A. G.; Fabiani, F. P. A.; Parsons, S.; Murrie, M.; Perlepes, S. P.; Brechin, E. K. *Inorg. Chem.* **2006**, *45*, 5281. (e) Krieck, S.; Goerls, H.; Westerhausen, M. *J. Organomet. Chem.* **2009**, *694*, 2204. (f) Dimitrou, K.; Sun, J.-S.; Folting, K.; Christou, G. *Inorg. Chem.* **1995**, *34*, 4160. (g) Pettersen, A.; Lennartson, A.; Hakansson, M. *Organometallics* **2009**, *28*, 3567.
(29) (a) Tanase, S.; Aromi, G.; Bouwman, E.; Kooijman, H.; Spek, A. L.; Reedijk, J. *Chem. Commun.* **2005**, *25*, 3147. (b) Viciano-Chumillas, M.; de Ruiter, G.; Tanase, S.; Smits, J. M. M.; de Gelder, R.; Mutikainen, I.; Turpeinen, U.; de Jongh, L. J.; Reedijk, J. *Dalton Trans.* **2010**, *39*, 4991.
(30) McNaught, A. D.; Wilkinson, A. *IUPAC: Compendium of Chemical Terminology*; 2nd Edition, 1997.
(31) (a) Palenik, G. J. *Inorg. Chem.* **1997**, *36*, 122. (b) Brese, N. E.; O'Keeffe, M. *Acta Crystallogr., Sect. B: Struct. Sci.* **1991**, *B47*, 192.
(32) Addison, A. W.; Rao, T. N.; Reedijk, J.; Van Rijn, J.; Verschoor, G. C. *J. Chem. Soc., Dalton Trans. Inorg. Chem.* **1984**, *7*, 1349.
(33) See the Supporting Information.
(34) Kambe, K. *J. Phys. Soc. Jpn.* **1950**, *5*, 48.
(35) Davidson, E. R. *GRID*; Indiana University: Bloomington, IN, 1999.
(36) (a) Vincent, J. B.; Christmas, C.; Chang, H.-R.; Li, Q.; Boyd, P. D. W.; Huffman, J. C.; Hendrickson, D. N.; Christou, G. *J. Am. Chem. Soc.* **1989**, *111*, 2086. (b) Saha, A.; Thompson, M.; Abboud, K. A.; Wernsdorfer, W.; Christou, G. *Inorg. Chem.* **2011**, *50*, 10476.
(37) (a) Aromi, G. S.; Claude, J.-P.; Knapp, M. J.; Huffman, J. C.; Hendrickson, D. N.; Christou, G. *J. Am. Chem. Soc.* **1998**, *120*, 2977. (b) Aromí, G.; Knapp, M. J.; Claude, J.-P.; Huffman, J. C.; Hendrickson, D. N.; Christou, G. *J. Am. Chem. Soc.* **1999**, *121*, 5489.
(38) (a) Stamatatos, T. C.; Poole, K. M.; Foguet-Albiol, D.; Abboud, K. A.; O'Brien, T. A.; Christou, G. *Inorg. Chem.* **2008**, *47*, 6593. (b) Stamatatos, T. C.; Foguet-Albiol, D.; Poole, K. M.; Wernsdorfer, W.; Abboud, K. A.; O'Brien, T. A.; Christou, G. *Inorg. Chem.* **2009**, *48*, 9831.